applied sciences

MDPI

Article

Impact Analysis and Optimization of Key Material Parameters of Embedded Water-Stop in Tunnels

Lin Wang [1], Chao Guan [2,*], Yimin Wu [1] and Chengkui Feng [3]

[1] School of Civil Engineering, Central South University, Changsha 410075, China; 214812312@csu.edu.cn (L.W.); wuyimin531@csu.edu.cn (Y.W.)
[2] China Railway 21st Bureau Group the 3rd Engineering Co., Ltd., Xianyang 712000, China
[3] Hubei Communications Planning and Design Institute Co., Ltd., Wuhan 430051, China; fck181205107232023@163.com
* Correspondence: valistill@163.com

Abstract: Leakage diseases frequently occur in mountain tunnels, and the lining joints are weak waterproof links. In order to solve the problems such as insufficient waterproof technology for existing tunnel joints, this paper relies on the scientific and technological project of the Hubei Provincial Department of Transportation to optimize the key parameters of the tunnel water-stop material and uses numerical simulation methods to analyze the impact of the hardness of the water-stop and the bond strength between the water-stop and concrete on its deformation and waterproof ability. Through the adhesion test, the optimization method of the bond strength between the water-stop and concrete is explored. The results show that: (1) the deformation stress of the water-stop will increase with the increase in hardness and reducing the hardness of the water-stop can improve its stress deformation state. Considering that low hardness increases the risk of damage and reduces the quality, it is recommended that the hardness be 55–60 (HA). (2) The adhesion between the water-stop and the concrete lining is the key to waterproofing the water-stop. Increasing the adhesion between the water-stop and the concrete is an effective optimization method. However, to prevent excessive deformation stress, it is necessary to optimize the geometric structure of the water-stop simultaneously. (3) Placing an epoxy–quartz sand coating on the surface of the water-stop can increase the adhesive force between the water-stop and the concrete. When the thickness of the epoxy layer is 2 mm, and the particle size of quartz sand is 26–40 mesh, the effect is best.

Keywords: tunnel engineering; water-stop; tunnel joints; epoxy−quartz sand coating; adhesion

check for updates

Citation: Wang, L.; Guan, C.; Wu, Y.; Feng, C. Impact Analysis and Optimization of Key Material Parameters of Embedded Water-Stop in Tunnels. *Appl. Sci.* **2023**, *13*, 8468. https://doi.org/10.3390/app13148468

Academic Editors: Zhongsheng Tan and Xiuying Wang

Received: 13 June 2023
Revised: 14 July 2023
Accepted: 20 July 2023
Published: 22 July 2023

1. Introduction

During tunnel construction, seepage water can not only delay construction progress but also cause serious accidents such as tunnel collapse [1], bringing great difficulties and safety hazards to the construction. In addition, seepage water adversely affects the safety and durability of tunnel lining [2], as well as the service life of tunnel facilities [3,4]. At the same time, seepage water can also deteriorate the environment inside the tunnel and seriously affect traffic [5], making it one of the main factors causing problems during tunnel operation [6,7]. Therefore, waterproofing is crucial to tunnel engineering, and lining joints are an important cause of water leakage. To prevent leaks at the joint, water-stops are generally installed in engineering projects to block water [8]. A water-stop is a strip made and installed to prevent water infiltration. It utilizes the high elasticity and compressive deformation of rubber to generate elastic deformation under various loads, thereby tightening and sealing, effectively preventing water leakage and seepage of building components.

Currently, there is no clear regulation in China regarding the selection of waterproofing measures for highway tunnel joints, while the joint waterproofing measures for railway tunnels include embedded water-stops, back-adhesive water-stops, waterproof sealing materials, etc. Generally, the selection should be based on the waterproofing grade. When the waterproofing grade is higher than level three, a combination of multiple waterproofing measures should be used, among which the embedded water-stop is a mandatory measure [9].

Since the successful development of rubber water-stops [10], polymer material water-stops have become the mainstream of water-stops. Rubber and plastic are the main materials of water-stops, with rubber being the primary one. There are many types of composite material water-stops, including steel-edged rubber water-stops compounded with rubber and metal, rubber water-stops embedded with metal mesh, and other [11] compounded water-stops. Therefore, the existing water-stop materials are mainly rubber-based and diverse and have become relatively mature after a long period of development.

However, in practical engineering, the expected waterproofing effect of water-stops is often difficult to achieve [12]. Yandong Jie et al. [13] indicate that the poor adhesion between rubber and concrete results in the waterproofing effect of water-stops, which is mainly generated from two aspects: one is enhancing the seepage resistance, and the other is prolonging the seepage path. Minqing Zhang et al. [14] have proposed that construction difficulties are the main reasons for the poor quality of tunnel joint waterproofing, including the low stiffness of rubber water-stops and the complexity of installation techniques. To address this issue, they proposed a new type of embedded water-stop with higher stiffness and transverse internal reinforcement. Byoung Hooi Cho, Weibin Ma, and Xiaoxiong Guo et al. [15–18] believe that improving the adhesion between water-stops and concrete can effectively improve their waterproof performance.

In this paper, the commonly used embedded water-stop in engineering is taken as the research object. The mechanism of the water-stop is introduced, and the influence of the material hardness and the adhesion between the water-stop and concrete on its deformation stress state are analyzed through finite element simulation. Furthermore, an optimization experiment on the bond strength between the water-stop and concrete is conducted.

2. Optimization of Key Parameters for Water-Stop Materials

2.1. Failure Mechanism of Embedded Water-Stop

Mountain tunnel circumferential joints are generally divided into two types: deformation joints and construction joints [19,20], and the embedded water-stop is set in the middle of the lining thickness along the circumferential direction. Under normal working conditions, due to the deformation of the lining, the embedded water-stop at the deformation joint is usually in a state of uneven settlement or expansion. The service life of rubber is closely related to its stress and strain, composition, and environment [21,22]. Its waterproof principle mainly includes two aspects: seepage resistance and seepage flow path.

Seepage resistance is composed of contact pressure and adhesion force formed by extrusion sealing. When the other variable is not considered, the water pressure is greater than the contact pressure, or the water pressure is greater than the bonding force, then leakage occurs, as shown in Figure 1.

When considering both factors simultaneously, as the water pressure increases, the contact pressure first fails, and then the bonding force begins to bear the pressure. As the failure occurs, the joint leaks water [8]. The seepage flow path can consume groundwater head pressure and enhance the waterproof reliability of the water-stop.

When the deformation of the water-stop is large, the stress may exceed the critical stress value. Being in a state of high stress for a long time will cause the mechanical properties of the water-stop to decline rapidly, reducing its service life and leading to waterproof failure before reaching the expected service life. Deformation can also damage the bond, decreasing the water-stop waterproofing performance.

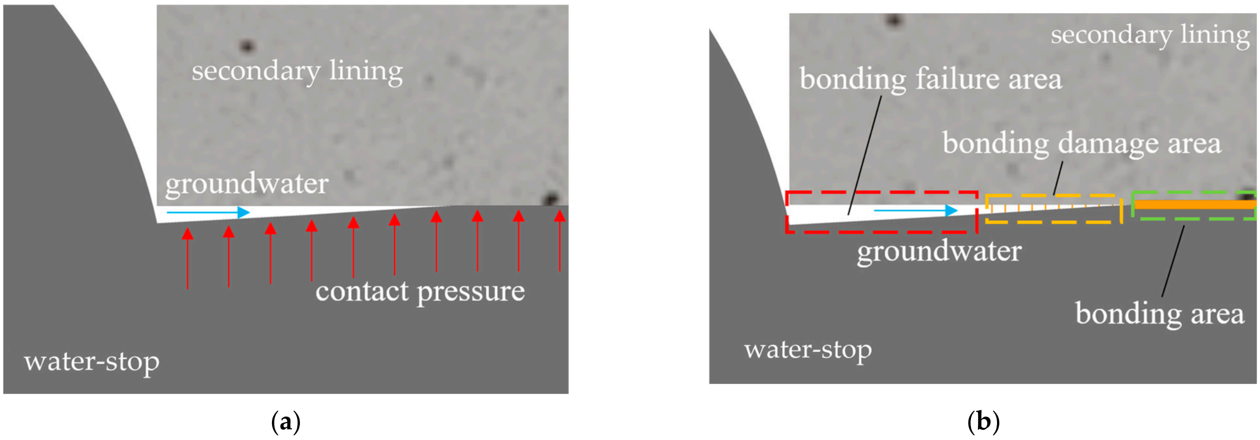

Figure 1. Waterproofing mechanism of water-stop. (**a**) extrusion sealing. (**b**) bonding water plugging.

When the stress level of synthetic rubber and other polymers does not exceed 20% of their tensile strength [23], their service life can reach more than 100 years. From the specifications, the tensile strength of rubber water-stops should be more than 10 MPa. In order to determine whether the rubber material fails during the service of tunnel joint water-stops, a critical stress value of 2 MPa can be used for the study of lining joint water-stops [23,24].

2.2. Finite Element Model

According to the adhesive force test of pure rubber and concrete test blocks, the normal adhesive force, tangential adhesive force, cohesive force parameters and so on were measured. In order to analyze the influence of water-stop hardness and the bonding force between the water-stop and concrete on its stress state, a finite element model of an embedded water-stop is established using the finite element software ABAQUS/Standard 2020. The embedded rubber water-stop is simulated using the Mooney-Rivlin model, with dimensions as shown in Figure 2. The concrete damage plasticity model is used to simulate the tunnel lining, considering the grade of the concrete as C30, the modulus of elastic E_C as 30 GPa, and the Poisson's ratio ν_c is 0.2. The concrete damage plasticity model in ABAQUS is used to simulate the failure of the lining. In the damage plasticity parameters, the eccentricity e_f, the ratio of biaxial to uniaxial compressive strength f_{b0}/f_{c0}, and the coefficient k are set to 0.1, 1.16, and 0.667, respectively. Based on the implicit solution of ABAQUS, the viscosity parameter μ_c needs to be set to 0.005. The dilation angle ψ is set to 30°. The stress–strain curves of concrete are determined according to the Code for the design of concrete structures [25]. The dimensions are 300 mm in width and 400 mm in height.

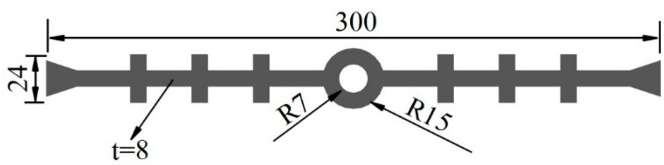

Figure 2. Water-stop dimensions (mm).

According to the specifications, the hardness of the rubber water-stop in the tunnel joint is 60 ± 5, and the hardness of rubber in this paper is Shore hardness (HA). In this simulation, the middle value of 60 is taken for calculation. Based on experience, the value of C_{01}/C_{10} is generally taken as 0.25 for better fitting. The calculated values are $C_{10} = 0.483$ MPa and $C_{01} = 0.121$ MPa.

The contact between the water-stop and the concrete is set as a normal hard contact, and the tangential direction uses the penalty function method with a friction coefficient of

0.3. Cohesive contact is also considered, with a normal stiffness of 3860, tangential stiffness of 1510, normal cohesive force of 0.386 MPa, and tangential cohesive force of 0.151 MPa. The plastic displacement is 0.0009 mm. Self-contact is set for the holes in the water-stop, with a friction coefficient of 0.8. It is assumed that the construction quality of the water-stop is great, and the finite element model is shown in Figure 3.

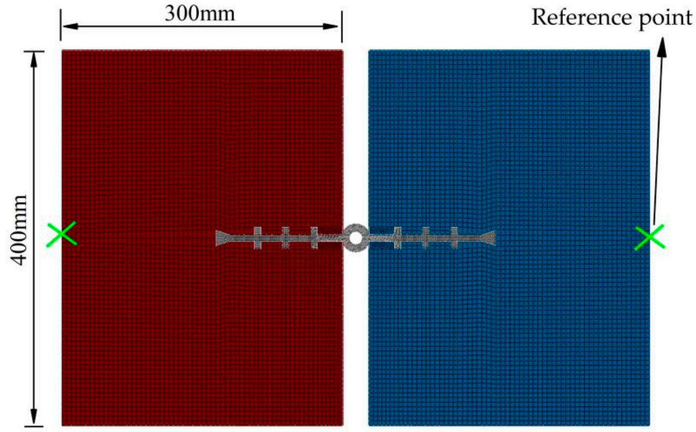

Figure 3. Finite element analysis model.

For the deformation of the lining, a reference point is coupled with the concrete in the model, and deformations in various directions are applied to the reference point to simulate the settlement, elongation, and compression of the lining. The maximum limits for deformation, tension and compression can be taken to 30 mm, 20 mm, and 10 mm, respectively.

2.3. Analysis of the Influence of Water-Stop Hardness on Its Deformation Force State

Hardness is the ability of a material to resist local penetration by a hard object on its surface, and it is a comprehensive indicator of the mechanical properties of a material, such as elasticity, plasticity, strength, and toughness. The specifications have made clear provisions for the hardness of some waterproof materials: for water-swelling rubber strips, the specifications stipulate a hardness range of 32–58; for rubber sealing gaskets, the specifications stipulate a hardness range of 50–70; and for rubber water-stops, the specifications stipulate a hardness range of 60 ± 5.

To explore the influence of different hardness on the force deformation of water-stops, a wider hardness range than specified in the specifications is selected, and different water-stop hardness values are set. The rubber parameters are shown in Table 1. A plane strain finite element model of embedded water-stops is established using ABAQUS/Standard.

Table 1. Material parameters of rubber water-stops.

Working Condition	Hardness/HA	E_0/MPa	C_{10}/MPa	C_{01}/MPa
1	40	1.696	0.226	0.057
2	45	2.045	0.273	0.068
3	50	2.465	0.329	0.082
4	55	2.978	0.397	0.099
5	60	3.619	0.483	0.121
6	65	4.443	0.592	0.148
7	70	5.542	0.739	0.185
8	75	7.080	0.944	0.236
9	80	9.388	1.252	0.313

The calculation results of the deformation stress of the water-stops are shown in Figures 4–6. It can be observed from the results that:

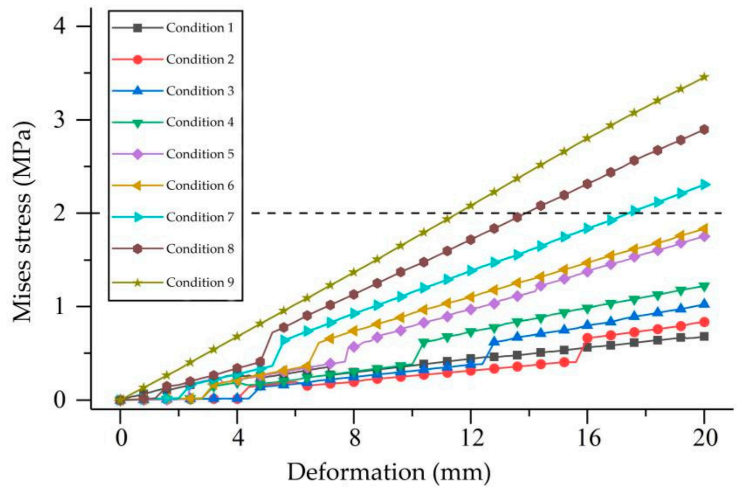

Figure 4. Tensile deformation stress of water-stops with different hardness.

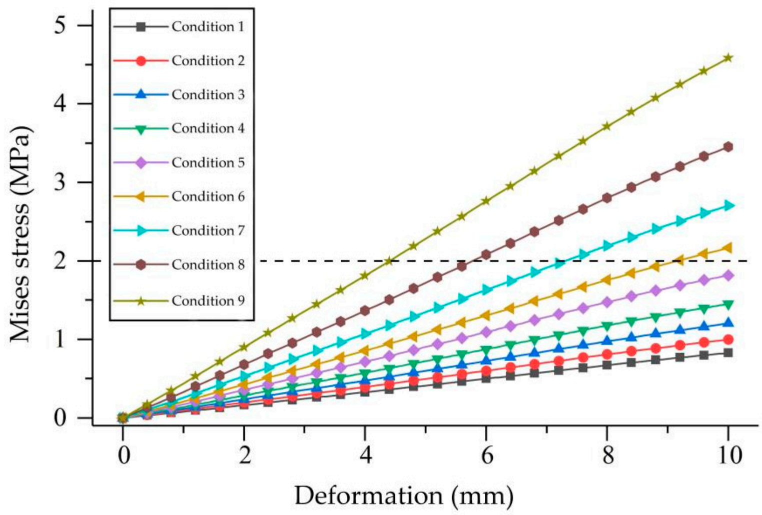

Figure 5. Compressive deformation stress of water-stops with different hardness.

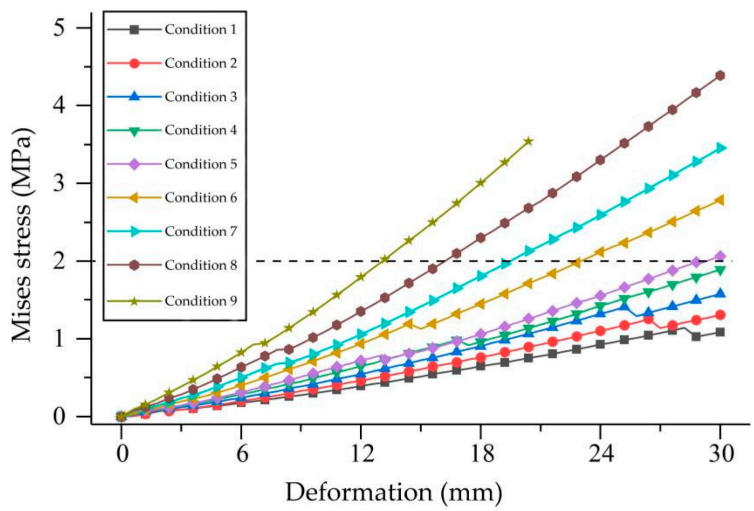

Figure 6. Settlement deformation stress of water-stops with different hardness.

① During tensile deformation, the deformation stress of the water-stop increases with the increase in hardness, and the deformation stress exceeds the dangerous stress value when the hardness exceeds 70 in working condition 7;

② During compressive deformation, the deformation stress of the water-stop increases with the increase in hardness, and the deformation stress exceeds the dangerous stress value when the hardness exceeds 65 in working condition 1;

③ During settlement deformation, the deformation stress of the water-stop also increases with the increase in hardness, and the deformation stress exceeds the dangerous stress value when the hardness exceeds 60 in working condition 5. At the same time, after working condition 7, when the hardness reaches 70, the settlement deformation of the water-stop causes tensile damage to the concrete lining, as shown in Figure 7. With the increase in hardness, the tensile damage value DAMAGET of the concrete lining changes from 0.667 to 0.998 (when the hardness of the water-stop is 80, i.e., in working condition 9, only part of the curve is shown in the figure due to excessive concrete damage).

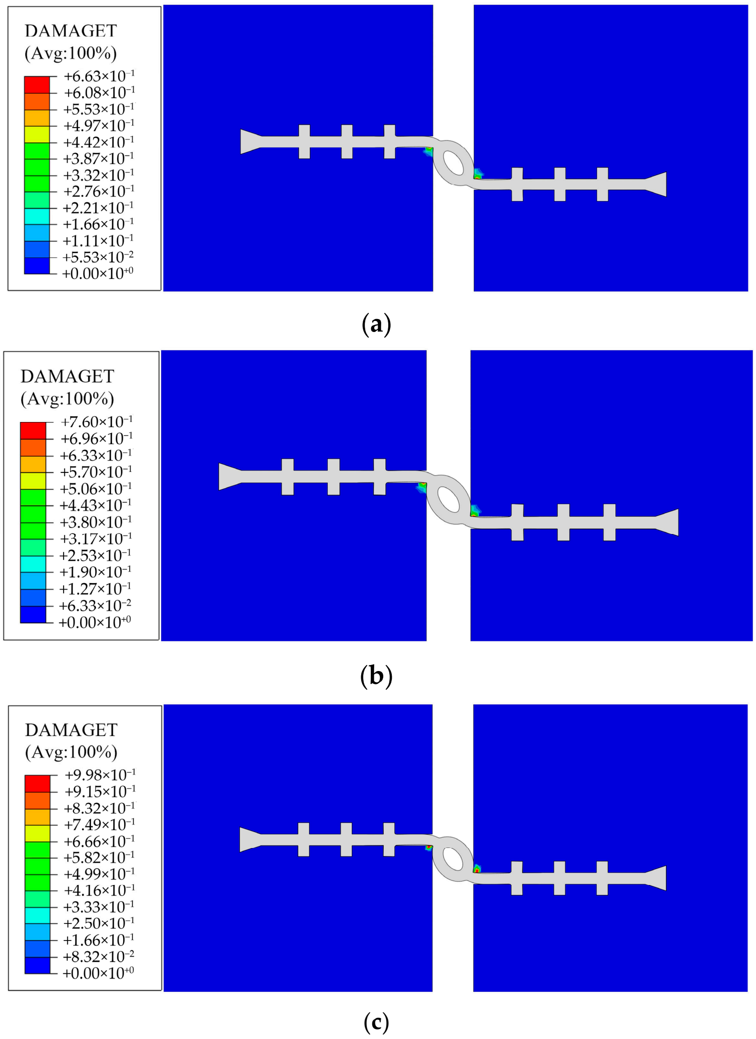

Figure 7. Settlement deformation concrete lining stiffness damage cloud map. (**a**) Working condition 7. (**b**) Working condition 8. (**c**) Working condition 9.

From the above analysis, it can be concluded that the deformation stress of the water-stop will increase with the increase in the material hardness of the water-stop. When the hardness of the water-stop reaches 60, the settlement deformation stress exceeds the dangerous stress value; when the hardness of the water-stop reaches 65, the compressive deformation stress exceeds the dangerous stress value; when the hardness of the water-stop reaches 70, the tensile deformation stress exceeds the dangerous stress value. At the same time, when the hardness of the water-stop reaches 70, the settlement deformation will cause tensile damage to the concrete lining. Therefore, it can be considered that a lower material hardness of the water-stop has a certain effect on improving the deformation stress of the water-stop.

In conclusion, although reducing the hardness of the water-stop can improve its stress deformation state, the hardness of the water-stop is a comprehensive indicator of its mechanical properties and the ability to resist hard objects pressing into its surface. If the hardness of the water-stop is too low, it may cause damage to the water-stop during construction or service, and the risk of the water-stop being torn or punctured is higher. Secondly, when the hardness of the water-stop is low, i.e., softer, it may cause difficulties in installation and positioning during construction, increasing the construction difficulty and reducing the project quality. The hardness range of the water-stop specified in the code is 55~65; based on this, it is recommended that the hardness of the water-stop in the design should be 55~60.

2.4. Analysis of the Influence of the Bonding Property of Water-Stops on Their Deformation and Stress State

The waterproofing ability of water-stops depends on their surface contact pressure and bonding force. The contact pressure is difficult to change due to the structure; the waterproofing ability could be improved by increasing the bonding force of water-stops. To analyze the deformation and stress state of water-stops under different bonding forces, the bonding forces between rubber and concrete obtained from the tests are used as the basis, and different bonding forces are set, as shown in Table 2. A finite element model is established using ABAQUS/Standard, and the deformation is applied in the same way as described above.

Table 2. Rubber and concrete bonding force parameters.

Working Condition	Normal Adhesive Force/MPa	Tangential Adhesion Force/MPa
1	0.000	0.000
2	0.193	0.076
3	0.386	0.151
4	0.579	0.227
5	0.772	0.302
6	1.158	0.453
7	1.930	0.755
8	3.088	1.208

The calculation results of the water-stop deformation stress are shown in Figures 8–10. The results show that: ① During tensile deformation, the deformation stress of the water-stop exhibits significant fluctuations after working condition 6, with the deformation stress first increasing and then decreasing. Before working condition 7, the deformation stress eventually tends to approximate values, while the deformation stress in working condition 8 shows a significant increase; ② During compression deformation, the deformation stress curves of each working condition are almost identical, indicating that the compression deformation is mainly due to the concrete lining squeezing the pores of the water-stop, which hardly destroys the bond between the water-stop and the concrete. The size of the bond strength between the water-stop and the concrete has little effect on the compression deformation stress of the water-stop; ③ During settlement deformation, the deformation stress of the water-stop does not show an obvious regularity with the change in bond strength before working condition 6, while after working condition 6, a clear regularity is observed, with the deformation stress increasing with the increase in bond strength.

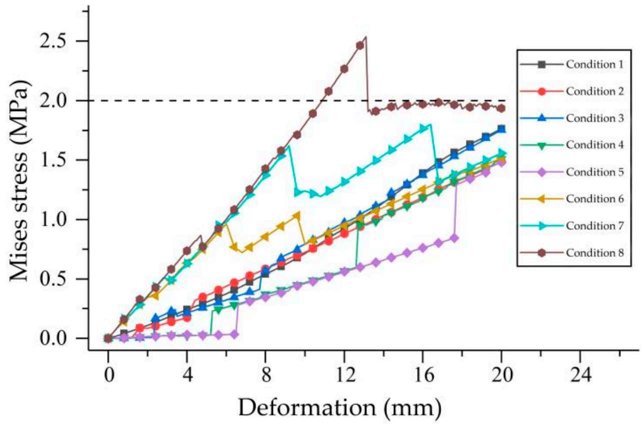

Figure 8. Tensile deformation stress of water-stop with different bonding forces.

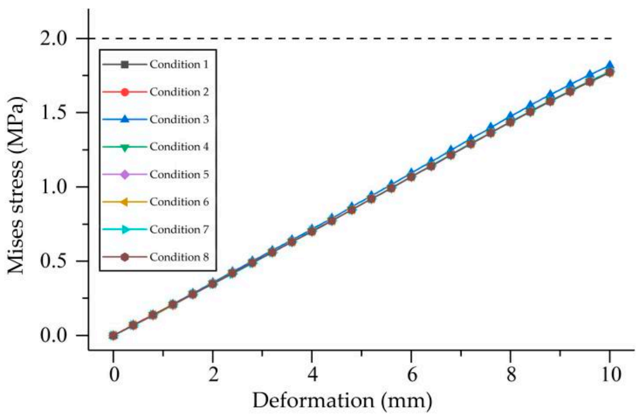

Figure 9. Compressive deformation stress of water-stop with different bonding forces.

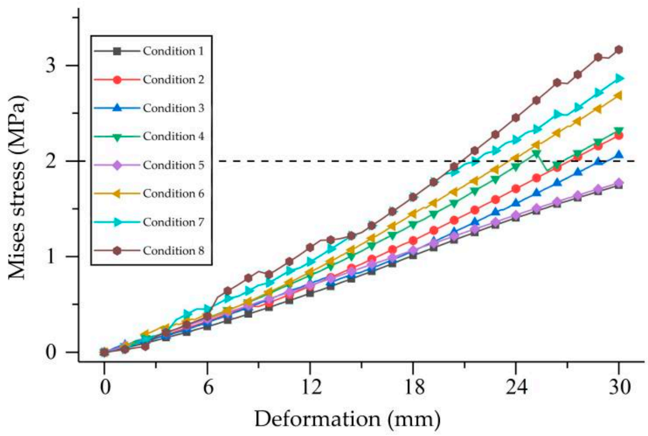

Figure 10. Settlement deformation stress of water-stop with different bonding forces.

From the above analysis, it can be concluded that the compression deformation stress of the water-stop is independent of the bond strength between the water-stop and the concrete. However, the tensile and settlement deformation of the water-stop exhibits different changing patterns, with working conditions 6 and 8 as the dividing points. To analyze the reasons for the appearance of the dividing points and further understand the relationship between the deformation stress of the water-stop and the bond strength between the water-stop and the concrete, further research should be conducted.

To further analyze the influence of bond strength on the stress state of water-stop deformation, research is conducted on the bond failure area between the deformed water-stop and the concrete lining. In Figure 11, the schematic diagrams of the bond failure area after the tensile deformation of the water-stops from Case 4 to Case 8 are shown. It can be seen from the figure that in Case 4 and Case 5, the bond failure area after deformation just covers the first water-stop rib on both sides (the bond failure area of the cases before Case 4 is similar). In Case 6 and Case 7, after the water-stop deformation, the bond failure area is between the first water-stop ribs on both sides, just at the edge of the water-stop ribs. After the deformation of Case 8, the bond failure area has the smallest range, and the water-stop ribs are not within the failure range.

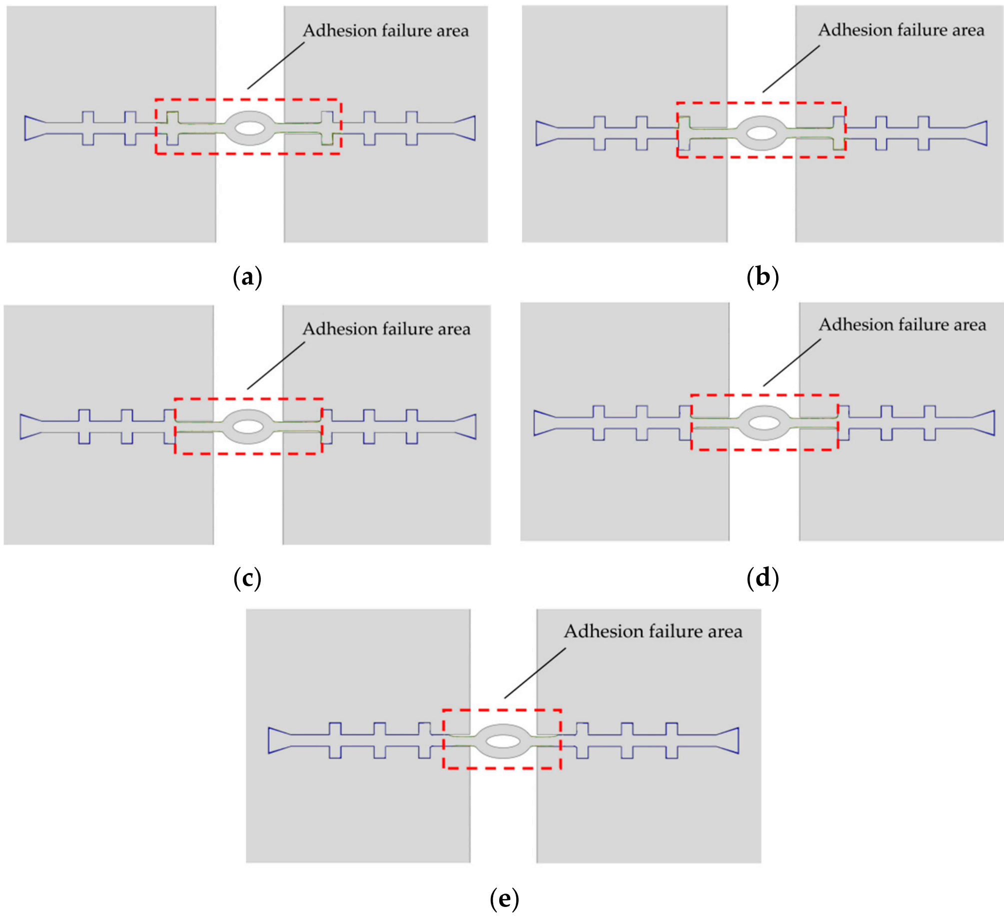

Figure 11. Bond failure area of partial working conditions in tensile deformation. (**a**) Working condition 4. (**b**) Working condition 5. (**c**) Working condition 6. (**d**) Working condition 7. (**e**) Working condition 8.

It can be concluded that after working condition 6, the bond strength between the water-stop and the concrete increases, and the bond failure range decreases (the bond of the water-stop ribs is not failed). In the process of stress, with the increase in deformation, the stress of the water-stop increases continuously before the bond failure between the wing plate and the concrete lining. Once the bond between the wing plate and the lining fails, the stress of the water-stop drops sharply, and then due to the next part of the bond not failing, the stress of the water-stop increases with the increase in deformation, and the change is more dramatic. Similarly, since the final stress is borne by the water-stop ribs after deformation, the stress of the water-stop deformation tends to be similar in all working conditions before working condition 7. In working condition 8, due to the excessive bond strength, the wing plate between the first water-stop ribs on both sides still bears the deformation, and the stress of the water-stop deformation is relatively large at this time.

Figure 12 shows the bonding failure area between the water-stop and concrete lining after settlement deformation for Cases 4 to 8. As the bonding strength increases, the bonding failure area gradually decreases. Before Case 6, the bonding failure area includes or is close to the water-stop ribs, and the water-stop ribs participate in the stress, so there is no obvious relationship between the water-stop deformation stress and the bonding strength at this time. However, after case 6, the bonding failure area is only within the water-stop wing, not including the water-stop ribs, so the water-stop deformation stress is relatively large at this time, and as the bonding strength increases, the water-stop deformation stress will continue to increase.

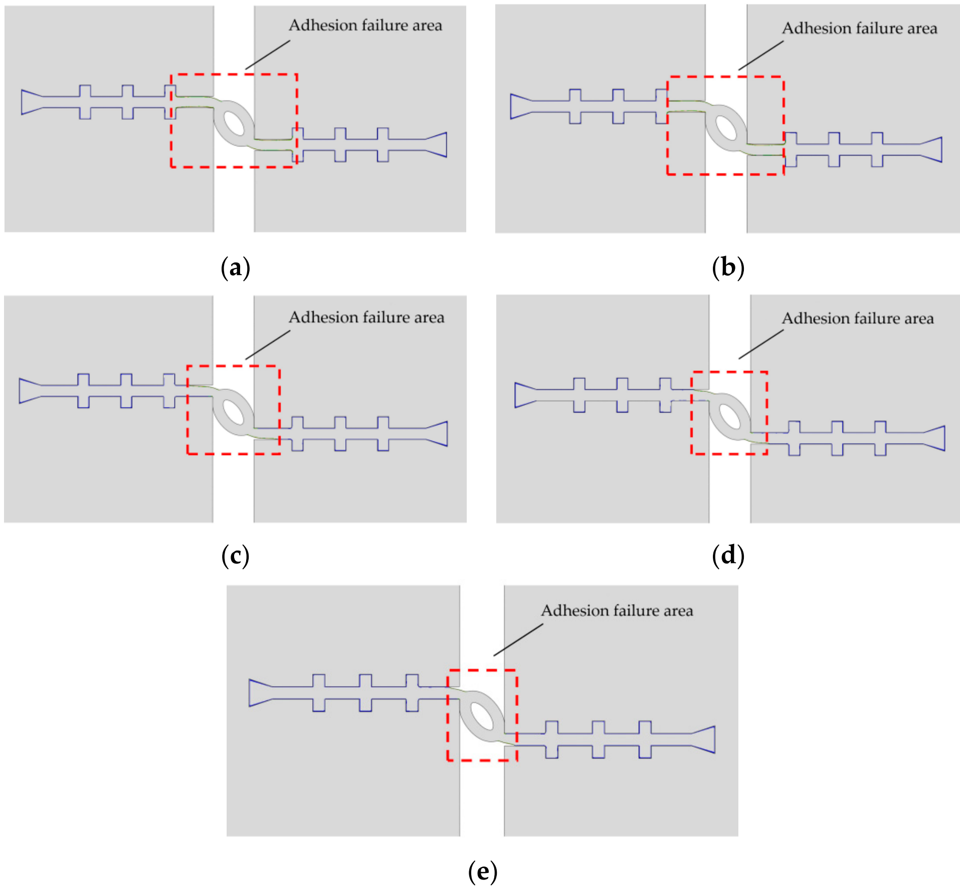

Figure 12. Bond failure area of partial working conditions in settlement deformation. (**a**) Working condition 4. (**b**) Working condition 5. (**c**) Working condition 6. (**d**) Working condition 7. (**e**) Working condition 8.

In summary, when the bonding force reaches a certain value, the bonding failure area between the water-stop and the concrete lining will decrease with the increase in the bonding force, except for the compressive deformation. The deformation stress of the water-stop will increase with the increase in the bonding force. When the bonding force is relatively large, the deformation stress of the water-stop exceeds the critical stress value. This indicates that increasing the bonding force between the water-stop and the concrete is an effective optimization method, but it may lead to excessive deformation stress of the water-stop. When carrying out such optimization, it should be combined with the optimization of the geometric structure of the water-stop.

3. Optimization of the Bonding between the Water-Stop and Concrete

As can be inferred from the above analysis, the optimization of the bonding between the water-stop and concrete should be limited to a certain range. According to previous research and engineering experience, it is believed that the bonding strength can be improved through various methods, such as ① Applying a self-adhesive layer like double-sided tape on the surface of the water-stop; ② Coating the water-stop surface with a layer that has strong bonding with concrete, such as epoxy–quartz sand; ③ Roughening the surface of the water-stop or creating grooves. Different methods have different effects on improving the bonding strength of the water-stop.

It is proposed to use epoxy–quartz sand coating to enhance the bonding strength between the water-stop and concrete. To investigate the enhancement effect of epoxy–quartz sand coating on the bonding strength and further analyze the influence of different epoxy resin thicknesses and quartz sand particle sizes on the bonding strength, it was decided to conduct bonding strength tests between rubber and concrete with different interfaces.

3.1. Experimental Scheme

In this experiment, quartz sand with particle size ranges of 16–26 mesh, 26–40 mesh, 40–80 mesh, and 80–120 mesh, commonly available epoxy resin, and natural rubber sheet materials were selected. Due to the small size of the specimens in this experiment, and the fact that the adhesion comes mainly from the adhesion of cement paste and rubber, the ordinary Portland cement blocks were used in this experiment, and the compressive strength was 42.5 MPa. After forming a coating of quartz sand and epoxy resin on the rubber sheet material, a mold was used to cast the cement onto the rubber specimens with the coating, forming 12 groups of specimens, as shown in Table 3. The strengths of the shear bond and the tensile bond are taken as evaluation indicators in this experiment.

Table 3. Epoxy-quartz sand coating parameters.

Working Condition	Thickness of Epoxy Resin (mm)	Quartz Sand Particle Size (mesh)
1	1	16–26
2	1	26–40
3	1	40–80
4	1	80–120
5	2	16–26
6	2	26–40
7	2	40–80
8	2	80–120
9	3	16–26
10	3	26–40
11	3	40–80
12	3	80–120

3.2. Specimen Preparation

Each group of specimens mentioned above contains three tensile bond strength and three shear bond strength specimens, resulting in a total of 72 specimens for this experiment. To obtain rubber-cement specimens under different working conditions, as shown in Figure 13, rubber sheets with dimensions of 200 mm × 200 mm × 20 mm were purchased. Due to the fluidity of epoxy resin before solidification, it is difficult to control the amount and thickness when directly applying it to the rubber sheet. To facilitate the application of epoxy resin, a mold was fabricated, as shown in Figure 14, which was used to fix and wrap the applied surface.

Figure 13. Rubber sheet.

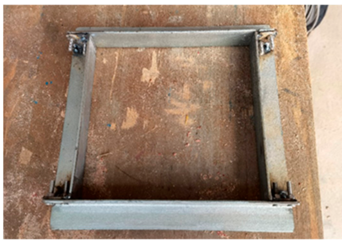

Figure 14. Epoxy–quartz sand coating mold.

After fixing and wrapping the rubber block with the epoxy–quartz sand coating mold, the thickness of the epoxy layer varies under different working conditions. To more accurately ensure the difference in epoxy layer thickness, the required epoxy amount was calculated based on the desired epoxy layer thickness and the area of the coating surface. Then, a beaker was used to measure the specified amount of epoxy resin. After stirring the measured epoxy resin evenly, the epoxy was applied to the cutting and tensile surfaces.

After the epoxy resin layer was applied, quartz sand with different particle sizes was sprinkled on the epoxy resin coating surface according to the needs of different working conditions. To achieve a better bond between the epoxy resin and the quartz sand, the sand should be spread slowly and evenly, completely covering the surface. After the quartz sand was basically leveled, it was gently pressed with a rubber plate. The completed specimen is shown in Figure 15.

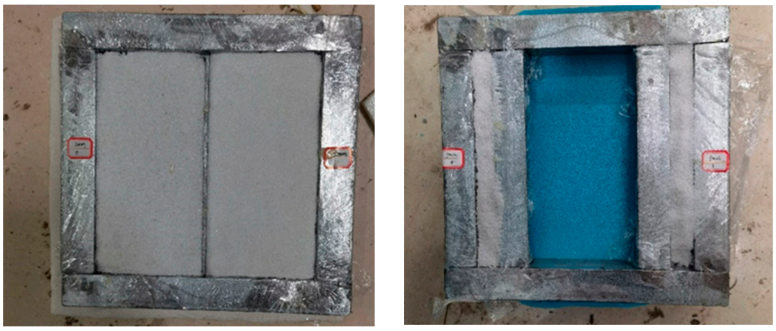

(**a**) (**b**)

Figure 15. Quartz sand coating. (**a**) section plane. (**b**) stretch plane.

After the epoxy–quartz sand layer on the rubber surface is set, the rubber sheet was cut into rectangular rubber blocks with dimensions of 100 mm $\times$ 50 mm $\times$ 20 mm. The epoxy–quartz sand coating on the tensile and shear surfaces of the rubber blocks under various working conditions is shown in Figure 16.

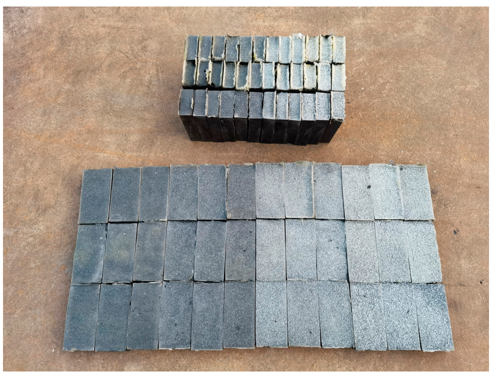

Figure 16. Rubber coating specimens for various working conditions.

After the completion of the epoxy–quartz sand coating on the rubber blocks, cement casting was carried out on the tensile and shear surfaces, respectively. The weight ratio of cement, sand, and water was 1:5.27:1.25, as shown in Figure 17. The size of the cement test blocks was 100 mm × 50 mm × 20 mm.

Figure 17. Cement casting.

After the epoxy–quartz sand coating of the rubber-cement specimens was completed, the tensile bond strength test surface was a rectangular area of 50 mm × 20 mm, and the shear bond strength test surface was a square area of 50 mm × 50 mm. Once the specimens were cast, they were placed in an environment with a temperature of 20 ± 2 °C and a relative humidity of 95% or higher for 28 days of curing. Some rubber-cement specimens under various conditions are shown in Figure 18.

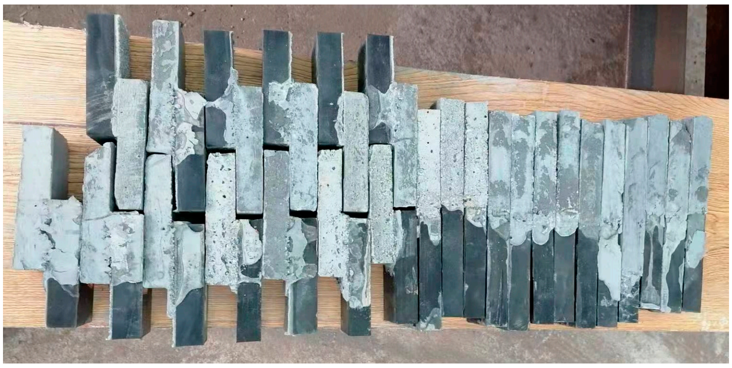

Figure 18. Casted rubber-cement coated specimens.

3.3. Test Method

The experimental equipment used was a tensile testing machine (0~5000 N), with specific fixtures to fix the specimens. The fixation of rubber-cement tensile and shear specimens is shown in Figure 19. Due to the rectangular shape of the rubber-cement specimens and the brittleness of the bonding interface, the selected tensile speed was 5 mm/min. The maximum stress sustained during the process of bonding failure caused by external forces was taken as the tensile or shear strength. The average strength of three specimens in each group was taken as the measured result.


(a)


(b)

Figure 19. Schematic diagram of specimen fixation. (**a**) tensile specimen. (**b**) shear specimen.

The tensile bond strength test results of the rubber-cement specimens are shown in Table 4 (the symbol "/" indicates that the cement block broke during the tensile process, and no specific value was measured). From the table, it can be seen that the tensile bond strength measured for conditions 1, 2, 5, 6, 7, 9, and 10 are all greater than 0.9 MPa, while the bond strength for the remaining conditions is less than 0.8 MPa and greater than 0.6 MPa. This indicates that the epoxy–quartz sand coating can indeed enhance the tensile bond strength between rubber and concrete. The degree of enhancement is relatively small concerning the thickness of the epoxy resin layer but more significant concerning the particle size of the quartz sand. When the thickness of the epoxy resin layer is 2 mm, the tensile bond strength is larger, and when the particle size of the quartz sand is larger (such as 40–80 mesh, 80–120 mesh), the tensile bond strength is smaller. Among them, the tensile bond strength of condition 6 is the largest.

Table 4. Tensile bond strength of cement-rubber coated specimens.

Working Condition	Test 1/MPa	Test 2/MPa	Test 3/MPa	Tensile Bond Strength/MPa
1	1.160	1.089	/	1.125
2	1.140	1.067	0.976	1.061
3	0.571	0.643	0.740	0.651
4	0.654	0.638	0.584	0.625
5	0.947	0.863	/	0.919
6	1.157	1.260	1.227	1.215
7	1.050	1.128	1.212	1.130
8	0.502	0.693	0.678	0.624
9	1.120	0.989	1.243	1.117
10	0.876	/	0.958	0.917
11	0.715	0.806	0.763	0.761
12	0.505	0.602	0.689	0.600

The shear bond strength test results of the rubber-cement specimens are shown in Table 5. It can be observed from the tables that the shear bond strength measured for conditions 1, 2, 5, 6, 7, 9, and 10 are all greater than 0.3 MPa, while the remaining conditions have bond strengths less than 0.3 MPa and greater than 0.2 MPa. This indicates that the epoxy–quartz sand coating can also enhance the shear bond strength. When the quartz sand particle size is larger, the bond strength is smaller, and when the epoxy resin layer thickness is 2 mm, the bond strength is larger. Among them, the shear bond strength of condition 6 is the largest.

Table 5. Shear bond strength of cement-rubber coated specimens.

Working Condition	Test 1/MPa	Test 2/MPa	Test 3/MPa	Shear Bond Strength/MPa
1	/	0.397	0.412	0.405
2	0.306	0.376	0.344	0.342
3	0.303	0.276	0.240	0.273
4	0.202	0.223	0.246	0.224
5	0.404	0.387	0.412	0.401
6	0.432	0.423	/	0.428
7	/	0.340	0.356	0.348
8	0.215	0.248	0.256	0.240
9	0.372	0.394	0.356	0.374
10	0.328	0.332	0.312	0.324
11	0.237	0.262	0.228	0.243
12	0.224	0.206	0.252	0.227

In summary, the epoxy–quartz sand coating on the surface of the water-stop can enhance the bonding strength between the water-stop and the concrete. There is a certain relationship between the thickness of the epoxy resin layer, the particle size of the quartz sand, and the enhancement of the bonding strength. When the thickness of the epoxy layer is 2 mm, and the particle size of the quartz sand is 26–40 mesh, the bonding strength is the greatest.

4. Conclusions

Based on the waterproof working mechanism of embedded water-stops, this chapter establishes finite element models of water-stops with different material parameters from the perspectives of water-stop hardness and the bonding force between water-stops and concrete lining. The effects of key material parameters on the stress and deformation of water-stops are analyzed, revealing the laws of the influence of water-stop hardness and the bonding force between water-stops and concrete lining on the stress and deformation of water-stops and their waterproof capacity. An optimization method for the bonding force between water-stops and concrete lining is proposed and verified through experiments. The main conclusions are as follows:

(1) Water-stop hardness is a comprehensive indicator of its mechanical properties, such as elasticity, plasticity, strength, and toughness. The stress deformation of the water-stop will increase with the increase in hardness. Reducing the hardness of the water-stop can optimize its stress deformation state. However, when the hardness of the water-stop is low, the risk of tearing and puncturing increases, the construction difficulty may also increase, and the engineering quality may decrease. The hardness of water-stops specified in the code is 55–65, so it is recommended that the hardness of water-stops be 55–60.

(2) In addition to compression deformation, when the bonding force reaches a certain value, the bonding failure area between the water-stop and the lining concrete will decrease with the increase in the bonding force. The stress deformation of the water-stop will increase with the increase in the bonding force. When the bonding force is large, the stress deformation of the water-stop will exceed the dangerous stress value. This indicates that increasing the bonding force between the water-stop and the concrete can not only improve the water seepage resistance of the water-stop but also improve the waterproof reliability of the water-stop. However, to prevent excessive deformation stress, it is necessary to optimize the geometric structure of the water-stop simultaneously.

(3) It is proposed to increase the bonding force between the water-stop and the concrete by applying an epoxy–quartz sand coating on the surface of the water-stop, and the coating with different epoxy thicknesses and quartz sand particle sizes is verified through experiments. The results show that this method can indeed increase the bond-

ing force between the water-stop and the concrete. When the epoxy layer thickness is 2 mm, and the quartz sand particle size is 26–40 mesh, the effect is the best.

Author Contributions: Conceptualization, Y.W.; methodology, L.W.; validation, L.W.; investigation, C.G.; resources, C.G.; data curation, L.W.; writing—original draft preparation, L.W.; writing—review and editing, C.G.; visualization, C.F.; project administration, Y.W. and C.F. All authors have read and agreed to the published version of the manuscript.

Funding: This research was funded by the Department of Transport of Hubei Province Science and Technology Project: 2020-186-2-5.

Institutional Review Board Statement: Not applicable.

Informed Consent Statement: Not applicable.

Data Availability Statement: All data are available from the author.

Conflicts of Interest: The authors declare no conflict of interest.

References

1. Li, D.Y.; Li, X.B.; Li, C.C.; Huang, B.R.; Gong, F.Q.; Zhang, W. Case studies of groundwater flow into tunnels and an innovative water-gathering system for water drainage. *Tunn. Undergr. Space Technol.* **2009**, *24*, 260–268. [CrossRef]
2. Muhammad, N.Z.; Keyvanfar, A.; Abd Majid, M.Z.; Shafaghat, A.; Mirza, J. Waterproof performance of concrete: A critical review on implemented approaches. *Constr. Build. Mater.* **2015**, *101*, 80–90. [CrossRef]
3. Zhou, Z.Q.; Li, S.C.; Li, L.P.; Shi, S.S.; Xu, Z.H. An optimal classification method for risk assessment of water inrush in karst tunnels based on grey system theory. *Geomech. Eng.* **2015**, *8*, 631–647. [CrossRef]
4. Sañudo, R.; Miranda, M.; García, C.; García-Sanchez, D. Drainage in railways. *Constr. Build. Mater.* **2019**, *210*, 391–412. [CrossRef]
5. Yuan, Y.; Jiang, X.; Lee, C.F. Tunnel waterproofing practices in China. *Tunn. Undergr. Space Technol.* **2000**, *15*, 227–233. [CrossRef]
6. Peng, L.J. Existing operational railway tunnel water leakage causes and remediation technologies. *Adv. Mater. Res.* **2014**, *1004*, 1444–1449. [CrossRef]
7. Li, S.C.; Zhou, Z.Q.; Li, L.P.; Xu, Z.H.; Zhang, S.S. Risk assessment of water inrush in karst tunnels based on attribute synthetic evaluation system. *Tunn. Undergr. Space Technol.* **2013**, *38*, 50–58. [CrossRef]
8. Wu, Y.M.; Wu, H.P.; Chu, D.H.; Feng, S.; Zhang, J.J.; Wu, H.R. Failure Mechanism Analysis and Optimization Analysis of Tunnel Joint Waterstop Considering Bonding and Extrusion. *Appl. Sci.* **2022**, *12*, 5737. [CrossRef]
9. *TB 10003-2016*; Code for Design of Railway Tunnel. Chinese Railroad Publishing House: Beijing, China, 2017.
10. Xu, Q.H. Current Situation and Development of Rubber Water Stop Belt. *China Rubber* **2002**, *10*, 22–25.
11. Roy, K.; Debnath, S.C.; Potiyaraj, P. A critical review on the utilization of various reinforcement modifiers in filled rubber composites. *J. Elastomers Plast.* **2020**, *52*, 167–193. [CrossRef]
12. Liu, W.W.; Zhang, Z.C. Discussion on construction technology of installing embedded rubber waterstop belt in joints of railway tunnel lining. *Railw. Eng.* **2014**, *12*, 40–42. [CrossRef]
13. Xie, Y.D.; Lv, Z.Q.; Liu, P.Z. Optimization of Waterproof Construction Technology for Lining Structural Joints of Water-rich Mountain Tunnel. *Highway* **2020**, *65*, 151–155.
14. Zhang, M.Q.; Li, S.H.; Liu, J.C. Research and Development of the Embedded Rubber Waterstops Reinforced with Horizontally Built-in Steel Plates. *Mod. Tunn. Technol.* **2019**, *56*, 52–56. [CrossRef]
15. Cho, B.H.; Nam, B.H.; Seo, S.; Kim, J.; An, J.; Youn, H. Waterproofing Performance of Waterstop with Adhesive Bonding Used at Joints of Underground Concrete Structures. *Constr. Build. Mater.* **2019**, *221*, 491–500. [CrossRef]
16. Ma, W.B.; Guo, X.X.; Ma, C.F.; Guo, Y.; Jin, J.K.; Li, P. Structural Design and Performance Test Study of Self-adhesive Water Stop Belt. *China Railw.* **2015**, *11*, 30–33. [CrossRef]
17. Guo, X.X.; Ma, W.B.; Ma, C.F.; Guo, Y.; Jin, J.K.; Chen, S.J. Model test study on comprehensive waterproofing and drainage effect of self-stick water-stop belt. *Railw. Eng.* **2016**, *01*, 25–28.
18. Guo, X.X. Experimental Research on Anchoring Performance of Rubber Waterstop in Railway Tunnel. *Railw. Eng.* **2017**, *57*, 49–51.
19. Liu, X.Z.; Guo, B.; Li, X.F.; Sang, Y.L. Model Experiment Study on Effect if Deformation Joints on Road Tunnel Resisting Destruction By Thrust Fault Stick-slip Dislocation. *Chin. J. Rock Mech. Eng.* **2015**, *34*, 3837–3843. [CrossRef]
20. Wang, Z.Q.; Lei, Z.Y. Waterproof performance of non-curable rubber modified asphalt material at deformation joints. *Aust. J. Civ. Eng.* **2022**, *20*, 130–146. [CrossRef]
21. Qiu, X.W.; Yin, H.S.; Xing, Q.C. Research progress on fatigue life of rubber materials. *Polymers* **2022**, *14*, 4592. [CrossRef]
22. Kang, W.; Liu, J.F.; Xiong, W.; You, T.Y.; Wang, X.X.; Zeng, K.X.; Deng, Y.A.; Guo, Z.C.; Yuan, K. Basic mechanical and fatigue properties of rubber materials and components for railway vehicles: A literature survey. *Rev. Adv. Mater. Sci.* **2022**, *61*, 587–610. [CrossRef]
23. Gu, G.C. Mechanical analysis of rubber and plastic water-stop. In *National Sixth Geosynthetics Conference Proceedings*; Modern Knowledge Publishing House: Beijing, China, 2004; pp. 399–406.

24. *GB 18173.2-2014*; Polymer Water-Proof Materials—Part 2: Waterstop. Standards Press of China: Beijing, China, 2014.
25. *GB 50010-2010*; Code for Design of Concrete Structures. China Architecture & Building Press: Beijing, China, 2010.